Direct Detection of Products from the Pyrolysis of 2-Phenethyl Phenyl Ether

Mark W. Jarvis,*,† John W. Daily,‡ Hans-Heinrich Carstensen,§ Anthony M. Dean,§ Shantanu Sharma,|| David C. Dayton,⊥ David J. Robichaud,† and Mark R. Nimlos†

National Renewable Energy Laboratory, 1617 Cole Blvd., Golden, Colorado 80401, United States, University of Colorado at Boulder, Department of Mechanical Engineering, Boulder, Colorado 80309, United States, Colorado School of Mines, Department of Chemical Engineering, Golden, Colorado 80401, United States, Materials and Process Simulation Center, California Institute of Technology, Pasadena, California 91125, United States, and Research Triangle Institute, Research Triangle Park, North Carolina 27709, United States

Received: August 12, 2010; Revised Manuscript Received: October 29, 2010

The pyrolysis of 2-phenethyl phenyl ether (PPE, $C_6H_5C_2H_4OC_6H_5$) in a hyperthermal nozzle (300−1350 °C) was studied to determine the importance of concerted and homolytic unimolecular decomposition pathways. Short residence times (<100 μs) and low concentrations in this reactor allowed the direct detection of the initial reaction products from thermolysis. Reactants, radicals, and most products were detected with photoionization (10.5 eV) time-of-flight mass spectrometry (PIMS). Detection of phenoxy radical, cyclopentadienyl radical, benzyl radical, and benzene suggest the formation of product by the homolytic scission of the $C_6H_5C_2H_4-OC_6H_5$ and $C_6H_5CH_2-CH_2OC_6H_5$ bonds. The detection of phenol and styrene suggests decomposition by a concerted reaction mechanism. Phenyl ethyl ether (PEE, $C_6H_5OC_2H_5$) pyrolysis was also studied using PIMS and using cryogenic matrix-isolated infrared spectroscopy (matrix-IR). The results for PEE also indicate the presence of both homolytic bond breaking and concerted decomposition reactions. Quantum mechanical calculations using CBS-QB3 were conducted, and the results were used with transition state theory (TST) to estimate the rate constants for the different reaction pathways. The results are consistent with the experimental measurements and suggest that the concerted retro-ene and Maccoll reactions are dominant at low temperatures (below 1000 °C), whereas the contribution of the $C_6H_5C_2H_4-OC_6H_5$ homolytic bond scission reaction increases at higher temperatures (above 1000 °C).

Introduction

The pyrolysis behavior of phenyl ethers has been studied by researchers to elucidate pyrolysis of low rank coal and lignin from biomass.[1−3] 2-Phenethyl phenyl ether (PPE, **1**) was first suggested by Klein and Virk[3,4] as a model compound for the pyrolysis of lignin since the β-ether linkage of PPE represents about 50% of the interunit linkages found in lignin, one of the three biopolymers that constitute all biomass feedstocks.[5,6] From their work and subsequent studies there arose some uncertainty about the initial decomposition of this molecule. This uncertainty partially stems from the fact that direct experimental observation of the initial reaction products has often been difficult, particularly for radical channels.

There have been four proposed routes for the initial decomposition of PPE as shown in reactions 1−4 below. The first two reactions are homolytic bond dissociations in either the α-position, reaction 1, or the β−position, reaction 2. The primary products from these reactions are the free radicals 2-phenylethyl radical, **2**, and phenoxy radical, **3**, from reaction 1 and benzyl radical, **4**, and anisyl radical, **5,** from reaction 2. The reverse of reactions 1 and 2 are barrierless radical recombination reactions, so there are no saddle points on the potential energy surface (PES) for these reactions. The last two reactions are concerted elimination reactions involving a 6-centered transition state, **6**, the so-called "retro-ene" (Hoffmann[7]) reaction, shown in reaction 3, and a 4-centered transition state, **9**, called the Maccoll elimination,[8] shown in reaction 4. Both of these produce styrene, **7**, whereas the other product from reaction 3 is 2,4-cyclohexadienone, **8**, and that from reaction 4 is phenol, **10**.

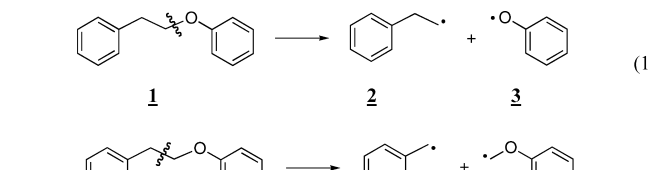

(1)

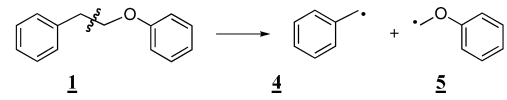

(2)

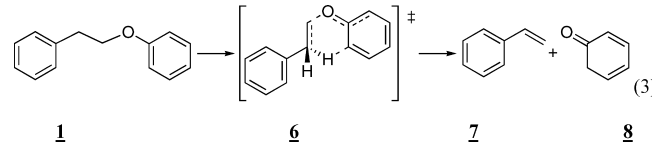

(3)

Klein and Virk[3,4] conducted pyrolysis experiments of neat PPE and PPE in tetralin, a hydrogen donor, from 300 to 500 °C in stainless steel bombs. They primarily measured phenol and styrene. Upon the basis of the similarity of products and kinetics in the presence of tetralin, they proposed that the retro-

* To whom correspondence should be addressed. E-mail: mark.jarvis@nrel.gov. Phone: 303 384-6376. Fax: 303 384-6103.
† National Renewable Energy Laboratory.
‡ University of Colorado at Boulder.
§ Colorado School of Mines.
|| California Institute of Technology.
⊥ Research Triangle Institute.

10.1021/jp1076356
Published on Web 01/10/2011

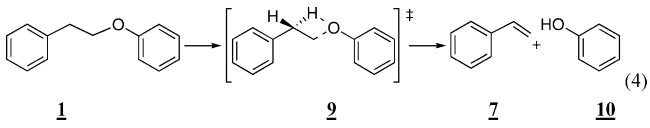

(4)

1 9 7 10

ene mechanism, reaction 3, best explained the observed data, but they suggested that homolysis mechanisms may play a minor role in PPE pyrolysis.

Britt et al. have more recently conducted extensive studies of PPE pyrolysis.[9,10] They explored the thermal decomposition of PPE, **1**, in constant volume reactors from 330−425 °C, for 5−40 min in the liquid phase and 5−480 min in the gas phase.[10] They also conducted flash vacuum pyrolysis experiments with PPE and methoxy substituted derivatives at 500 °C and a residence time of approximately 10 ms.[9] Again they observed phenol and styrene as major products. They proposed that C−O homolysis, reaction 1, was the dominant mechanism for PPE decomposition and that the retro-ene mechanism was minor based upon an analysis of experiments with deuterated isotopomers. It was suggested that phenol is formed from hydrogen abstraction reactions involving the phenoxy radical, **3**.

Estimation of the energetics for reactions 1−4 suggests that retro-ene reaction should be dominant until very high temperatures. The bond dissociation energy for reactions 1 and 2 can be estimated from group additivity[11] and known thermodynamics[12−17] to be $DH_{298}(C_6H_5O-CH_2CH_2C_6H_5) = 69$ kcal mol^{-1} and $DH_{298}(C_6H_5CH_2-CH_2OC_6H_5) = 76$ kcal mol^{-1}. As mentioned above, these reactions are not likely to proceed via pronounced barriers on the PES, therefore the bond dissociation energies may serve as approximations to the activation energies. Bond scission reactions such as these typically have large pre-exponential factors (10^{14} to 10^{16} s^{-1}). The kinetic parameters for the concerted reactions can be estimated based upon measured values for similar reactions. The retro-ene reactions have been measured for decomposition of alkyl vinyl ethers. For instance, the retro-ene dissociation of ethyl vinyl ether, reaction 5, has been measured and the reported activation energy[18] is $E_{a(5)} = 42.3 \pm 1.3$ kcal mol^{-1} with a pre-exponential factor[18] of $A_{(5)} = 10^{12.1\pm0.3}$ s^{-1}. The Maccoll elimination, reaction 4, can be approximated by the parameters for the reaction of diethyl ether to give ethanol and ethylene, reaction 6. The reported activation energy[19] for this reaction is $E_{a(6)} = 66$ kcal mol^{-1}, and the pre-exponential factor[19] is $A_{(6)} = 7.9 \times 10^{13}$ s^{-1}. From these values, the rate constants for reactions 1−4 can be estimated and are plotted as a function of temperature in Figure 1. On the basis of these rate constants, the retro-ene reaction is favored with rate constants orders of magnitude larger than the other reactions at 400 °C but is lower than the C−O homolysis reaction at temperature greater than 1250 °C.

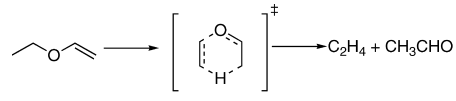

(5)

11 12

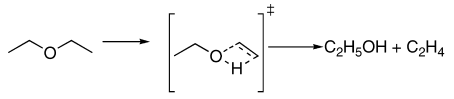

(6)

13 14

In this study we have used a hyperthermal nozzle to pyrolyze PPE and to isolate the initial products in a molecular beam for detection with photoionization mass spectrometry (PIMS). In order to help interpret the results for the PPE pyrolysis experiments, we have also conducted pyrolysis experiments with phenyl ethyl ether, PEE, **15**, which can undergo analogous reactions to PPE, reactions 7−9. However, in this case C−C homolysis is much less likely. Since PEE is smaller, we were also able to measure the products using matrix isolation Fourier Transform Infrared (FTIR) spectroscopy. Finally, we have conducted quantum mechanical calculations in order to determine which reactions are more likely and identify possible secondary reactions.

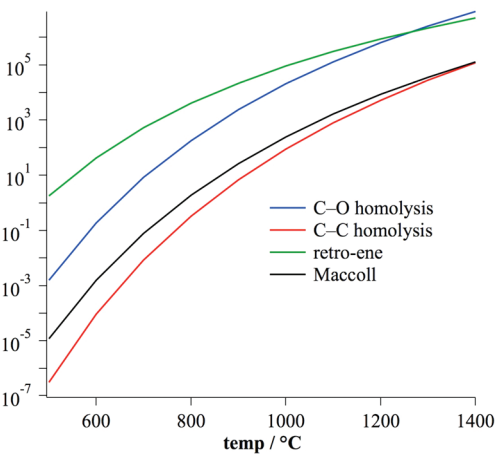

Figure 1. Rate constants for PPE decomposition derived from literature values for similar reactions. For k_1 Arrhenius parameters were taken from anisole dissociation, $C_6H_5OCH_3 \rightarrow C_6H_5O + CH_3$; $A_{(1)} = 2 \times 10^{15}$ s^{-1}, $E_{a(1)} = 64$ kcal mol^{-1}. For k_2 the A factor was estimated to be similar to k_2 and the activation energy was assumed to be the C−C bond enthalpy; $A_{(2)} = 1 \times 10^{15}$ s^{-1}, $E_{a(2)} = 76$ kcal mol^{-1}. For k_3, the constants from reaction 5 were used with a statistical multiplier of 4/3; $A_{(3)} = 1.7 \times 10^{12}$ s^{-1}, $E_{a(3)} = 42$ kcal mol^{-1}. For k_4 the constants from reaction 6 were used with a statistical multiplier of 2/3; $A_{(4)} = 5.3 \times 10^{13}$ s^{-1}, $E_{a(4)} = 66$ kcal mol^{-1}.

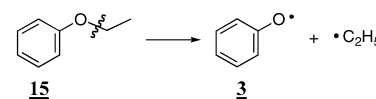

(7)

15 3

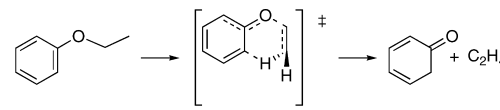

(8)

15 16 8

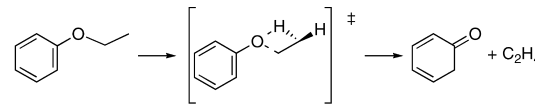

(9)

15 17 10

Experimental Section

To directly measure the primary products of the reactions shown in reactions 1−4 we used an experimental approach that has proven successful for measuring radicals and unstable pyrolysis products. The approach, Figure 2, has been described in detail elsewhere[20−23] and involves the pyrolysis of molecules in a resistively heated SiC nozzle and the measurement of the products with PIMS and matrix-IR spectroscopy. A Series 9 Parker General Valve pulsed the molecule of interest diluted in helium or argon into the hyperthermal nozzle, a resistively heated, 1 mm i.d. silicon carbide tube. The temperature on the

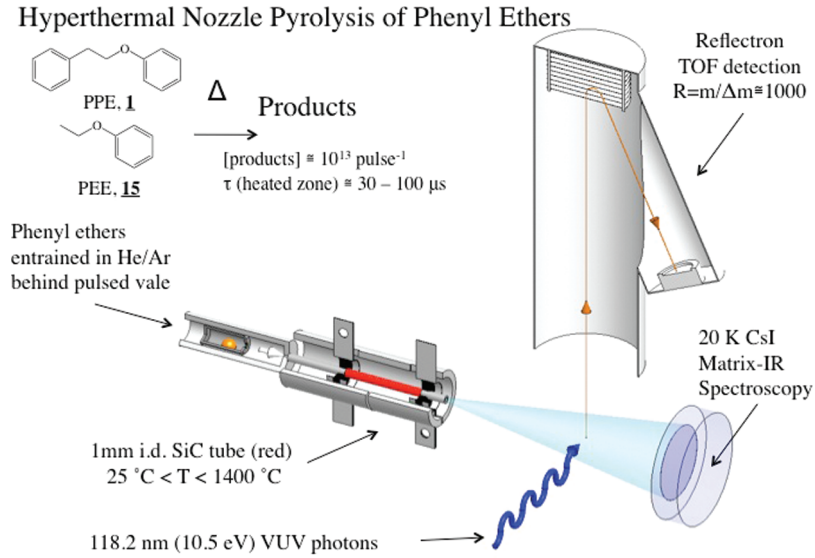

Figure 2. Schematic of experimental apparatus showing the hyperthermal nozzle, TOF section of the PIMS and matrix-IR components.

outside of the tube was monitored with a tungsten−rhenium thermocouple,[24] and the temperature was controlled by adjusting the current through the SiC tube. The electrode spacing determined the length of the hot zone in the reactor (2 cm) and the residence time of the gas in the tube has been estimated to be less than 100 microseconds.[20,21] At the end of the reactor, the gas expanded into the vacuum, quenching the reactions. Due to the short residence times, high temperatures, and low substrate to carrier ratio (<1:1000) secondary reactions were generally inhibited. As such, this reactor is useful for isolating radicals and reaction intermediates.[20,22,25−30]

In the PIMS apparatus,[31] the products from the hyperthermal nozzle in helium were ionized with vacuum ultraviolet (VUV) photons and detected with a reflectron time-of-flight mass spectrometer. The adiabatic expansion from the nozzle was skimmed and the pulsed molecular beam intersected a pulsed 118 nm (10.5 eV) VUV ionizing beam (10 Hz). The VUV photons were generated by tripling the third harmonic of an Nd:YAG laser (Continuum) in a xenon/argon cell.[20] Ions were detected at the end of the time-of-flight tube with a microchannel plate, and the signal was collected with a LeCroy 9350A 500 MHz digital oscilloscope. Typically, 5000 spectra were averaged for each temperature. Propylene and NO were used as calibration standards for the mass scale of the time-of-flight mass spectrometer. They were introduced into the vacuum chamber through the hyperthermal nozzle at room temperature (25 °C).

In the matrix isolation experiments, the products from the pulsed hyperthermal nozzle in an argon flow were deposited on a cryogenic CsI window and spectra were collected with an FTIR. The cryostat was a two-stage, closed-cycle helium refrigerator (APD Model HC-2) and the temperature at the end of the coldfinger (∼10 K) was measured with a silicon thermocouple. The CsI matrix window was mounted to the bottom of the coldfinger, approximately 2.5 cm from the outlet of the hyperthermal nozzle. Infrared spectra from 400−4000 cm^{-1} were collected using a FTIR spectrometer (ThermoNicolet Magna-IR Series II 550 Spectrometer) with a KBr beamsplitter and a MCT/B detector. At least 500 scans, with a resolution of 0.25 cm^{-1}, were collected for each condition. Background spectra of the cold window, prior to deposition of the matrix, were collected before each run, and these were used to calculate absorbance.

Experimental investigation of the primary unimolecular decomposition reactions studied here required low concentrations to limit secondary reactions. PIMS experiments at higher substrate to helium ratios (1:50) resulted in a decrease in the observed formation of radicals. For instance, at these high concentrations we observe low ratios of phenoxy radical to phenol, *m*/*z* peaks 93 and 94, and cyclopentadienyl radical to cyclopentadiene, *m*/*z* peaks 65 and 66. This suggests that hydrogen abstraction reactions occur with radicals at these concentrations. The same high concentration effects were also observed in the matrix-IR experiments. For the results reported here, the dilution of PPE and PEE was low enough (≤1:1000) so that the observed ratios of these peaks were insensitive to changes in concentration. This suggests that at these concentrations, the hydrogen abstraction reactions were minimized. The vapor pressures of PPE and PEE were adjusted by heating the sample holder, and the values were estimated using the Lee−Kesler method as described by Reid et al.[32] We held the sample region temperature at 100 °C to produce 1 Torr PPE, **1**, in 2000 Torr helium. This was the lowest sample region temperature that resulted in an acceptable signal-to-noise ratio. For PEE, **15**, a slightly higher concentration of ∼3 Torr in 1500 Torr argon was needed to obtain acceptable spectra in the matrix-IR experiment. PPE, **1**, was obtained from Frinton Laboratories (99%) and PEE, **15**, was obtained from Sigma Aldrich (99%), and they were used after being degassed with freeze−pump−thaw cycles (liquid nitrogen). Room temperature mass spectra showed only peaks from the parent molecule, so the trace contaminants (if any) would have a negligible impact on the pyrolysis behavior.

Computational Section

Quantum mechanical electronic structure calculations were used to compare the energies of the competing decomposition pathways for PPE and PEE and to estimate the rates of the reactions. All calculations were carried out with the Gaussian 03 suite of programs[33] using the CBS-QB3 method. This method optimizes the geometry using density function theory (B3LYP) and then extrapolates to the complete basis set limit with MP2, MP4, and CCSD(T) single point calculations. A complete description of this method can be found in the literature.[34] This approach has been shown to produce a mean absolute error of 0.87 kcal mol^{-1} and absolute max error of 2.8 kcal mol^{-1} when compared to the G2 set of molecules. CBS techniques have also been found to produce reliable transition state energies.[35−38]

TABLE 1: Comparison of Relevant Experimental Energies to Results Obtained with CBS-QB3

	experimental (kcal mol^{-1})	CBS-QB3 (kcal mol^{-1})	expt ref
$DH_{298}(C_6H_5O-C_2H_5)$	70	68	76
$DH_{298}(C_6H_5O-CH_3)$	62 ± 3	62	77, 78
$DH_{298}(C_2H_3O-C_2H_5)$	65 ± 2	65	15, 79−81
$DH_{298}(C_2H_5O-C_2H_5)$	86 ± 1	88	13, 15, 82, 83
$DH_{298}(C_2H_5OCH_2-CH_3)$	85	87	13, 17, 84, 85
$DH_{298}(C_6H_5CH_2-CH_3)$	77.6 ± 0.6	79	13, 84, 86, 87
$E_{a(5)}$	42.3 ± 1.3	45	18
$E_{a(6)}$	66	68	19

Transition states were determined as those having a reasonable geometry with a single imaginary frequency, whose atomic displacement appeared to approximate the reaction coordinate. In addition, IRC calculations were conducted to establish that the transition state connected the reactant to the product.

In order to test the accuracy of the computational approach used in this study we compared the results from CBS-QB3 calculations to relevant experimental measurements. The homolytic unimolecular decomposition of PPE shown in reactions 1 and 2 will likely have monotonically increasing potential energy along the reaction coordinate. Thus, the transition state cannot be localized as a saddle point on the PES but needs to be determined as the location along the reaction coordinate where there is a minimum in the density of states of transverse modes. A suitable method to find this minimum (as a function of temperature) is variational transition state theory (vTST). However, as suggested by Beste and Buchanan,[39] PPE and the transition states of its reactions contain numerous vibrational modes with very low frequencies which, if not treated properly, lead to substantial uncertainties in absolute rate constants. These uncertainties are expected to be significantly larger for variationally determined rate constants of the barrierless homolysis reactions of PPE. Therefore, such an attempt is unwarranted unless a reliable code suitable for large molecules, such as PPE, was available. Development of a vTST code is beyond the scope of this study. Instead, we have employed the same strategy as Beste and Buchanan[40] and concentrate on the calculation of the bond dissociation energies alone. For these reactions, we have used the calculated bond dissociation energy, D_0, for the activation energy, E_a, and have selected experimental preexponential factors, A, from similar reactions. Because bond dissociation energies are difficult to measure, we have compared calculated bond dissociation enthalpies, DH_{298}, to experimental values for similar reactions to those shown in reactions 1 and 2. Several of these are presented in Table 1. Typically, the calculated values are within 1−2 kcal mol^{-1} of the uncertainty limits of the experimental values. As a test of our approach for reactions 3 and 4, we calculated the activation energies for reactions 5 and 6 and compared the results to experimental values. This is also shown in Table 1. The calculated energy barrier was determined by eq 1, where E is the potential energy, ZPE is the zero point energy determined using the calculated harmonic frequencies, TS is the transition state, and R is the reactant. As can be seen the calculated values are within 2 kcal mol^{-1} of the experimental values. The calculated energies for the molecules and transition states used to obtain the values in Table 1 are collected in the Supporting Information as are the Cartesian coordinates of the optimized structures. The results from these calculations suggest that an upper limit of the uncertainty in the bond dissociation energies and transition state energies is 2 kcal mol^{-1} for the molecules studied here.

$$E_{calc} = E_{TS} + ZPE_{TS} - E_R - ZPE_R \quad (1a)$$

In contrast to reactions 1 and 2, the retro-ene reaction, reaction 3, and the Maccoll reaction, reactions 4, proceed via pronounced energy barriers, which allows for an easy identification of the transition state geometries and application of canonical transition state theory[41,42] to calculate the corresponding rate expressions. In terms of the Gibbs free energy, the rate constants can be calculated according to eq 2:

$$k(T) = \kappa(T)k_B T/hV_m(n - 1)\exp(-\Delta G^{\#}/RT) \quad (2a)$$

Here, $\kappa(T)$ is the tunneling correction factor, V_m is the molar volume at standard pressure ($V_m = RT/p$, with $p = 1$ atm), n is the molarity of the reaction (e.g., $n = 1$ for unimolecular, $n = 2$ for bimolecular), and $\Delta G^{\#}$ is the difference in Gibbs free energy between the transition state geometry (ΔG^{TS}) and the reactant(s) (ΔG^{reac}),

$$\Delta G^{\#} = \Delta G^{TS} - \Delta G^{reac} = \Delta H^{TS} - T\Delta S^{TS} - \Delta H^{reac} + T\Delta S^{reac} \quad (3a)$$

All other symbols represent common parameters. The ΔG^{TS} term for the transition state does not include contributions from the reaction path mode (imaginary frequency vibration).

We calculate the entropies and heat capacities via well-established methods from statistical mechanics based on partition functions for the different energy modes in molecules. Heats of formation are obtained with the atomization energy method.[43] Since the TST method requires only energy differences, most systematic bond errors[44] that might be apparent will cancel out. Most of the internal modes are treated using the harmonic oscillator-rigid rotor approximation, and the B3LYP/CBSB7 frequencies of the CBS-QB3 method are scaled by a factor of 0.99 prior to their use. Some low frequency vibrations of molecules of interest in this work resemble rotations around a single bond (hindered rotations), and these internal rotations are treated separately using the following approach: First we determine the hindrance potential via a relaxed PES scan, in which the dihedral angle corresponding to the selected rotation is varied in steps of 10° until a full rotation of 360° is achieved. At each dihedral angle value all other degrees of freedom are allowed to vary until the energy is minimized. The obtained hindrance potential is fitted to a Fourier series. Second, we calculate the effective moment of inertia for the rotation. For symmetric rotors this value is easily calculated since the rotating axis coincides with the actual bond,[45] but for asymmetric rotors the calculation is more demanding. Kilpartick and Pitzer[46] solved this problem for the general case and East and Radom[47] provided practical approximate methods to calculate effective moment of inertias for internal rotations. We use their $I^{(2,3)}$ method in this work. Third, with the potential and effective moment of inertia in hand, we numerically solve the Schrödinger equation for a one-dimensional rotor. The obtained energy eigenvalues are finally used to calculate the partition function and contributions of this mode to the thermal energy, entropy, and heat capacity.

The temperature dependent transmission factor κ(T), which accounts for contributions from quantum mechanical tunnelling, is obtained from asymmetric Eckart potentials.[48] This method requires the magnitude of the imaginary frequency as well as the barrier heights in forward and reverse directions. All this

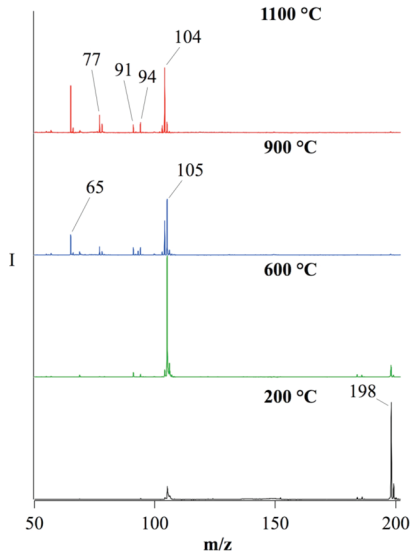

Figure 3. Mass spectra of the products of pyrolysis from PPE (1:2000) at select temperatures.

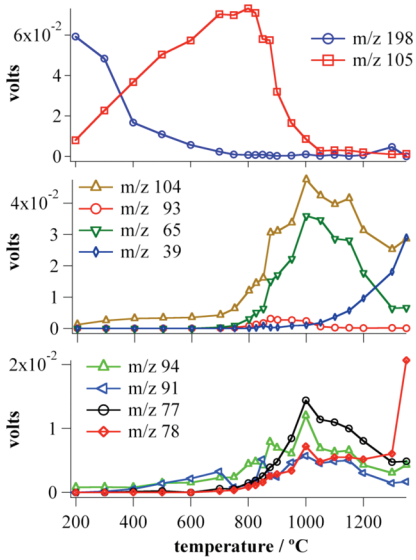

Figure 4. Plots of the intensity of the peaks in the mass spectra from the pyrolysis of PPE (1:2000) as a function of temperature.

information is readily available from the CBS-QB3 results for the reactants, products, and transition state.

Rate expressions are calculated with eq 2 in 50 K steps for the temperature interval 300−2500 K. The data set is then fitted to a modified Arrhenius expression,

$$k(T) = AT^n e^{-E/(RT)} \quad (4a)$$

Note that the "E" value defined in eq 4 differs from the activation energy "E_a" by $E = E_a - nRT$.

Results and Discussion

The mass spectra of pyrolysis products from PPE support the existence of the reactions shown in reactions 1−4. The mass spectra collected at nozzle temperatures of 200, 600, 900, and 1100 °C are shown in Figure 3, and plots of the intensities of individual ions as a function of temperature are shown in Figure 4. All vertical axes in the spectra are plotted on the same scale for comparison of relative intensities. As can be seen, at 200 °C the parent ion (m/z = 198) is prominent in the mass spectrum. As the nozzle is heated up to 600 °C the intensity of the parent decreases and a peak at m/z = 105 grows in. Although this peak could be due to phenyl ethyl radical, **2**, it is more likely that it is due to fragmentation during the photoionization process. At these low temperatures, thermal fragmentation of PPE is unlikely, and if it was significant, the other product from this reaction, phenoxy radical, **3** should be observed at m/z = 93. The spectra show only a very small peak at m/z = 93. Furthermore, the formation of phenyl ethyl radical is unlikely because loss of a hydrogen atom to form styrene, **7**, or loss of ethylene to form phenyl, **18**, as shown in reactions 10 and 11 are thermodynamically more facile than dissociation of PPE to form **2**, reaction 1. As mentioned above the estimated enthalpy for reaction 1[12] is $\Delta_{react(1)}H_{298}$ = 69 kcal mol^{-1} as compared[49] to $\Delta_{react(10)}H_{298}$ = 31 kcal mol^{-1} for reaction 10 and $\Delta_{react(11)}H_{298}$ = 37 kcal mol^{-1} for reaction 11. Our CBS-QB3 calculations predict values of $\Delta_{react(1)}H_{298}$ = 69 kcal mol^{-1}, $\Delta_{react(10)}H_{298}$ = 31 kcal mol^{-1}, and $\Delta_{react(11)}H_{298}$ = 39 kcal mol^{-1}. Rate parameters were calculated to be $E_{a(10)}$ = 36.7 kcal/mol and $A_{(10)} = 7.3 \times 10^{12}$ s^{-1} for reaction 10 and $E_{a(11)}$ = 40.1 kcal/mol and $A_{(11)} = 6.4 \times 10^{13}$ s^{-1} for reaction 11. (The Cartesian coordinates and energies are gathered in the Supporting Information.) Thus, if phenyl ethyl radical is formed it will instantaneously dissociate to form either styrene or phenyl radical. As the temperature in the nozzle increases from 200 to 600 °C, the observed increased fragmentation is due to increased internal energy of PPE in the ionization region due to inefficient cooling during the adiabatic expansion from the nozzle. This type of behavior has been observed in earlier studies of the pyrolysis of allyl iodide.[26]

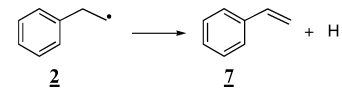

(10)

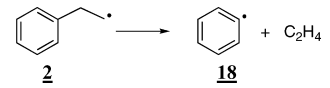

(11)

Evidence for C−O Homolysis. At 900 °C the peak at 93 is due to phenoxy radical, **3**, and is indicative of scission of the $PhCH_2CH_2$−OPh bond, reaction 1. As mentioned above, the other product from this reaction is phenyl ethyl radical, **2** (m/z = 105), which will quickly dissociate by reaction 10 to form styrene, **7** (m/z = 104). As can be seen in Figures 3 and 4, the peak at m/z = 104 grows in with increasing temperature. Also note that at 900 °C there is a peak at m/z = 65, which is due to the cyclopentadienyl radical, **19**, formed by reaction 12. Note, that we cannot observe CO from this reaction because the ionization energy[50] is greater than the laser energy, IP(CO) = 14.0142 ± 0.0003 eV. The activation energy[51] for this reaction is $E_{a(12)}$ = 43.9 ± 0.9 kcal mol^{-1}, but the transition state is tight and the pre-exponential factor[51] is small, $A_{(12)} = 2.5(\pm 1.5) \times 10^{11}$ s^{-1}. As a result the rate of removal of phenoxy radical by reaction 12 is nearly identical to the rate of formation of phenoxy radical by reaction 1 using the rate constants in Figure 1. For instance, the rate constant for reaction 1 at 900 °C is $k_{(1)} = 2.4 \times 10^3$ s^{-1}, whereas the rate constant for reaction 12 is $k_{(12)} = 2.4 \times 10^3$ s^{-1}. This is consistent with the experimental results presented in Figures 3 and 4, which show that intensity of the peak for phenoxy radical (m/z = 93) remains small with increasing temperature. Similar behavior for phenoxy radical and cyclopentadienyl radical has been observed from the

pyrolysis of anisole,[28,52] $C_6H_5OCH_3$, which produces phenoxy radical by the dissociation of the $C_6H_5O-CH_3$ bond.

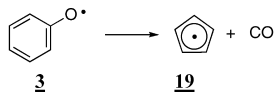

3 19 (12)

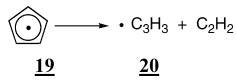

19 20 (13)

As the temperature increases the cyclopentadienyl radical decomposes to form propargyl radical, C_3H_3, $m/z = 39$, **20**, and acetylene as shown in reaction 13. Figure 4 show that the peak for propargyl radical strongly increases with temperature above 1000 °C. We cannot detect acetylene, C_2H_2 $m/z = 26$, because the ionization energy,[53] IP(C_2H_2) = 11.400 ± 0.004 eV, is greater than the energy of the ionizing photons. The rate for this reaction was calculated[54] using ROHF-CCSD(T) and RRKM, and the rate constant at 1 atm was fit with the following parameters, $A_{(13)} = 1.98 \times 10^{68}$ s^{-1}, $n_{(13)} = 15.0$, $E_{a(13)} = 124$ kcal mol^{-1}, where $k = AT^{-n} \exp(-E_a/RT)$. The calculated rate constant for this reaction is several orders of magnitude lower than the rate constant for reaction 12. For instance, at 900 °C, the calculated rate constant is $k_{(13)} = 1.4 \times 10^{-1}$ s^{-1}, four orders-of-magnitude lower than $k_{(12)}$, but at 1400 °C $k_{(13)} = 5.6 \times 10^3$ s^{-1} is only two orders-of-magnitude lower than $k_{(12)}$. The traces in Figure 4 show that the signal for propargyl radical, $m/z = 39$, increases with temperature above 1000 °C concomitantly with a decrease in the signal for cyclopentadienyl radical. The rate constants calculated for reactions 1 and 12 are high enough that above 1100 °C all of the PPE should be reacted and all of the phenoxy radical should be decomposed. This is consistent with the data shown in Figures 3 and 4. Growth of propargyl radical and loss of cyclopentadienyl radical are consistent with the growth in the calculated rate constant for reaction 13 relative to reaction 12. The observation that the peaks at $m/z = 65$ and $m/z = 39$ are dominant above 1100 °C is consistent with the proposition that the C−O homolysis reaction becomes a prominent decomposition pathway at the higher temperatures of this study.

At higher temperatures, 900−1200 °C, there is evidence for further decomposition of styrene, which can decompose to benzene, **22**, and acetylene as shown in reaction 14. The kinetics of this reaction have been studied in a shock tube,[55] and the derived pre-exponential factors and activation energy are $A_{(14)} = 1.58 \times 10^{11}$ s^{-1} and $E_{a(14)} = 58.4$ kcal mol^{-1}. Evidence for benzene is seen at $m/z = 78$ in the mass spectra. Acetylene can not be seen because its ionization potential[53] is greater than the energy of the ionizing photons. We have conducted separate experiments with styrene (Supporting Information) and the results from these tests show the same yield of the peak at $m/z = 78$, relative to styrene, as observed during PPE pyrolysis.

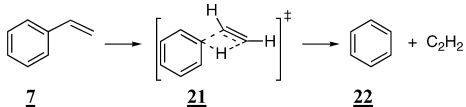

7 21 22 (14)

Evidence for C−C Homolysis. The small peak with m/z 91 is an indication of the homolysis of the $PhCH_2-CH_2OPh$ bond as shown in reaction 2. This m/z corresponds to the mass of benzyl radical and the accompanying anisyl radical product, $PhOCH_2$, **5**, has a mass 107. There was no significant signal obtained at $m/z = 107$ due to the rapid reaction of this species. The $PhOCH_2$ radical, **5**, will quickly undergo a 1,3-aryl shift to form the benzyloxy radical,[56] **23**, reaction 15. Reactions 16 and 17 show the dominant reactions for this radical. In reaction 16 hydrogen atom is eliminated to form benzaldehyde, **24**, and in reaction 17 formaldehyde is eliminated to form phenyl radical, **18**.[57,58] A third reaction, not shown, forming benzene and HCO is only predicted to account for 5−10% of the chemistry of the benzyloxy radical, **23**.[58] The PES for $PhOCH_2$, **5**, has been calculated at the CBS-QB3 level of theory and used to determine kinetic parameters for reaction 16 and 17. The activation energies and pre-exponential factors for reactions 16 and 17 have been calculated to be $E_{a(16)} = 19.5$ kcal/mol $A_{16} = 2.2 \times 10^{14}$ s^{-1} and $E_{a(17)} = 26.5$ kcal mol^{-1} $A_{17} = 5.9 \times 10^{14}$ s^{-1}. Kinetic modeling indicates the ratio of reaction 16 to reaction 17 to be approximately ∼7:1 at 900 °C (when taking into account photoionization cross sections this ratio would be ∼3.5:1). It is difficult to find evidence for these pathways in the current experiments. In the mass spectra (Figure 2), there are very small signals for $m/z = 106$ (the mass of benzaldehyde) once the natural abundance of $^{13}C_1$-isotopomers of $m/z = 105$ ($C_8H_9^+$) has been subtracted. However, benzaldehyde photofragments easily and therefore a significant signal at $m/z = 106$ would not be expected. Formaldehyde is not observable in our system due to its high ionization potential,[59] IP(CH_2O) = 10.88 ± 0.01 eV, and phenyl radical has a competing source from reaction 11, which should dominate.

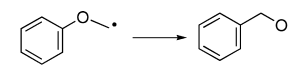

5 23 (15)

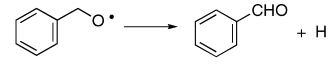

23 24 (16)

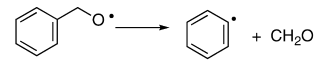

23 18 (17)

Evidence for Concerted Reactions. Evidence for the concerted reactions is provided by the presence of a peak in the mass spectrum at $m/z = 94$. This peak could arise from 2,4-cyclohexadienone, **8**, from reaction 3 or phenol, **10**, from reaction 4. However, it is more likely that the peak at $m/z = 94$ arises only from phenol. Any 2,4-cyclohexadienone that is formed from reaction 3 will be quickly converted to phenol by a 1,3 hydrogen transfer, keto−enol tautomerization, as shown in reaction 18. The barrier for this reaction has been calculated[60] to be low, $E_{a(18)} = 51$ kcal mol^{-1} with an associated rate constant of ∼9000 s^{-1} at 1000 °C. The reverse reaction has a much higher barrier of $E_{a(18\text{-rev})} = 69$ kcal mol^{-1}. It can therefore be calculated that at equilibrium there is less than 0.05% cyclohexadienone present. The other product from these reactions is styrene, but as shown above, styrene will also be formed from C−O homolysis, so $m/z = 104$ is not a distinguishing feature for the concerted reactions. To ensure that phenol did not originate from hydrogen abstraction reaction involving phenoxy radical, we conducted a number of experiments where the sample boat containing the PPE was heated from 100 to 150 °C and the mass spectra were measured. We estimate that the pressure of PPE in these experiments changed from about 1 to 8 Torr, with a mole fraction of 7×10^{-4} to 5×10^{-3}. Over this temperature

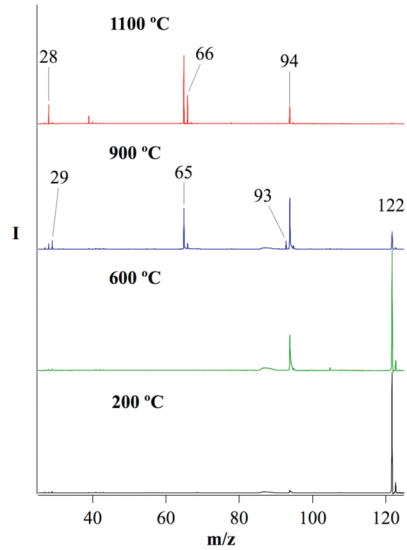

Figure 5. Mass spectra of the products from the pyrolysis of PEE (1:500) at select temperatures.

range, the intensity of $m/z = 94$ was linear with concentration, and there was little change in the ratio of the peak intensity of $m/z = 94$ to the intensity of $m/z = 93$. This suggests that in this pressure range, little phenoxy radical was reacting to give phenol. Since the rates for bimolecular reactions such as H abstractions depend quadratically on pressure (on the reactant concentrations) while the yields from unimolecular reactions at the high pressure limit depend only linearly on it, the 94/93 ratio should have clearly changed if H abstraction reactions played a role. The typical experiments described above were conducted with the valve held at a temperature of 100 °C, and these experiments suggest that hydrogen atom abstraction by phenoxy radical is not significant. A separate study was conducted[52] with anisole, **26**, using this experimental apparatus and similar concentrations, and the mass spectra contained only a small peak at $m/z = 94$; this was consistent with the isotopic ratio of $^{13/12}C$ of phenoxy radical arising from the C−O homolysis shown in reaction 19. This suggests that under these experimental conditions phenoxy radical will not form phenol through hydrogen atom abstraction. Thus, the $m/z = 94$ peak must arise from phenol formation due to reactions 3 or 4 or both.

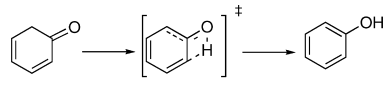

10 **25** **8** (18)

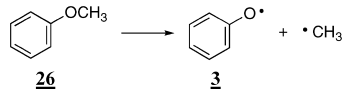

26 **3** (19)

Pyrolysis of PEE. The pyrolysis of PEE, **15**, produces mass spectra (Figure 5) that are consistent with the reactions shown in reactions 7−9 and so support the proposition that both homolytic bond scission and concerted reactions occur for PPE. At 600 °C the mass spectrum of PEE showed photofragmentation to give $m/z = 94$ and $m/z = 66$ in addition to the parent ion, $m/z = 122$. Reaction 7 shows the C−O homolysis reaction forming phenoxy radical and ethyl radical. Similar to 2-phenylethyl radical, **2**, ethyl radical, will rapidly undergo H atom loss to form ethylene. This bond dissociation enthalpy[58] is

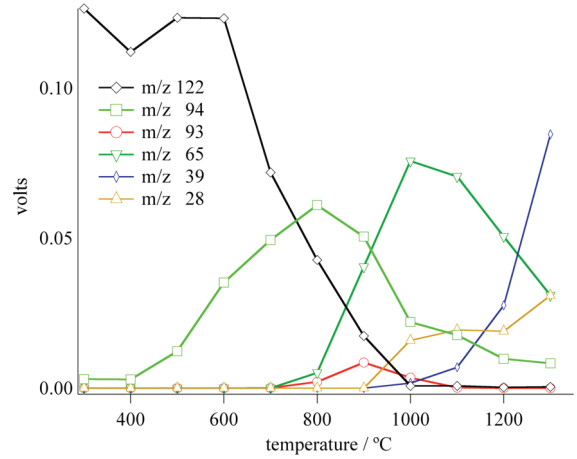

Figure 6. Plot of the intensities of the mass spectral peaks from the pyrolysis of PEE (1:500) as a function of temperatures.

$DH_{298}(CH_2CH_2-H) = 35.7 \pm 0.4$ kcal mol^{-1}. At 900 °C the mass spectra showed peaks at $m/z = 93$ and 65, which are phenoxy radical and cyclopentadienyl radical and are suggestive of the reaction 12. The peak at $m/z = 29$ is likely a photofragment of PEE similar to the $m/z = 105$ ion formed from PPE. Although the peak at $m/z = 94$ is a photofragment at low temperatures, at high temperatures, this peaks likely arises directly from decomposition of PEE. Compare the ion formation plots for PPE and PEE shown in Figures 4 and 6. Notice that the fragment ion of PPE, $m/z = 105$ in Figure 4a decreases rapidly to zero at 1000 °C, while the fragment ion from PEE, $m/z = 94$ in Figure 6a decreases toward zero at 1000 °C but then lingers on to higher temperatures. This is an indication that the peak at $m/z = 94$ is phenol formed from one of the concerted reactions for the decomposition of PEE shown in reactions 8 and 9. As with PPE, we cannot distinguish between the retro-ene products shown in reaction 8 and the Maccoll products shown in reaction 9. Note that both the concerted reactions and the C−O homolysis reaction will produce ethylene, which has an ionization potential,[61] $IP(C_2H_4) = 10.5138 \pm 0.0006$ eV, slightly larger than the nominal laser energy, ninth harmonic of Nd:YAG = 10.499 eV. The line width of the laser ($\sigma = 0.005$ eV) is sufficient that a small number of photons have energies above the ionization potential (1% are above 3σ more than the nominal energy). Thus, we observed a weak signal for ethylene, $m/z = 28$. This was confirmed in separate experiments with ethylene in helium, in which we also observed weak signals at $m/z = 28$. This ethylene signal could arise from reactions 7−9, and so, like styrene with PPE, this peak does not distinguish between these pathways.

The matrix isolation spectra of the pyrolysis of PEE show the formation of phenoxy radical and phenol, supporting the existence of reactions 7−9. These experiments were also conducted at a low concentration (1:1000) where the PPE experiments showed no evidence of bimolecular reactions. Bimolecular reactions were probed using higher concentrations (1:250 and 1:50), with the resulting spectra showing decreased phenoxy radical yield, increased phenol, and the appearance of cyclopentadiene. Figure 7 shows a typical IR absorption spectrum of the products from the pyrolysis of PEE in the hyperthermal nozzle. Initial products of the homolysis reaction, the phenoxy and ethyl radicals, were found to decompose to cyclopentadienyl radical plus carbon monoxide at higher temperatures and ethylene. No ethyl radical was observed in the matrix spectra. The assignments in the spectrum are based upon literature measurements and spectra of products measured

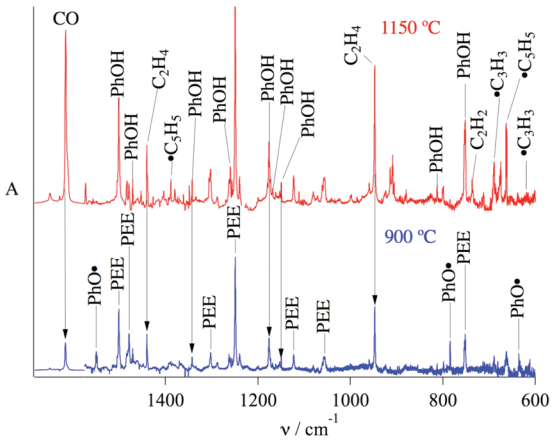

Figure 7. Matrix isolation spectrum of the products from the pyrolysis of PEE (1:1000). The assignments are based upon literature values and spectra collected in this study (see Table 2).

TABLE 2: Integral IR Absorbencies (Scaled to the Strongest Vibration for Each) of Phenyl Ethyl Ether Pyrolysis Products in a 20 K Argon Matrix (Right Columns), Comparison of Literature Values (Left Columns) to This Work[a]

species[ref]	ω (cm^{-1})	relative intensity	ω (cm^{-1})	relative intensity
phenoxy radical[88]	635	100.0	635	65.4
	784	72.1	784	52.0
	1550	63.0	1550	100.0
	1481	53.1	1481	69.6
	898	24.0	898	15.6
	1072	18.0	1072	27.6
phenol[89]	1176	100.0	1176	87.3
	1169	87.5	1169	9.1
	1603	87.5	1601	53.3
	1262	77.5	1262	21.2
	1501	67.5	1501	59.6
	751	65.0	752	61.2
	685.9	62.5	689.1	10.3
*[90]	3635*	62.5	3635	100.0
	1151	47.5	1150	22.8
ethylene[91]	946	vs	947	100.0
	1440	s	1440	22.2
	3111	m	3111	19.8
	2995	m	2995	7.4
	3081	w	3082	12.2
cyclopentadienyl radical[92]	661	vs	662	100.0
	1383	m	1383	17.1
	3079	w	3079	sh
carbon monoxide[93]	2138	vs	2138	vs
	2149.3	m	2149.3	m
propargyl radical[30]	3308.5	vs	3308.5	100.0
	686.6	m	686	51.6
	482	s	noise	noise
	620	m	620	39.4
acetylene[94]	736.2	vs	736	100.0
	3289	s	3288	12.2
	3302.5	m	3301	4.7

[a] vs = very strong, s = strong, m = medium, w = weak, and b = broad.

separately. The peak assignments are collected in Table 2, which also lists the molecular frequencies from the literature. The measured spectra for phenol and cyclopentadiene are shown in the Supporting Information.

Estimation of Rate Constants for Decomposition of PPE and PEE. We used the results from CBS-QB3 calculations to estimate rate constants for PPE and PEE decomposition. As mentioned above, for the homolysis reactions, we use the bond dissociation energy, D_0, as an estimate of the activation energy, E_a. For instance, for reaction 1 the activation energy was determined to be $E_{a(1)} = D_0 = E_0(C_6H_5O) + E_0(C_6H_5C_2H_5) - E_0(PPE)$, where E_0 is the calculated energy including zero point energy. The calculated activation energies for the homolysis reactions, (1), (2), and (7), are shown in Table 3. The pre-exponential factors, A, were estimated from similar reactions, because, as discussed previously, these reactions proceed via barrierless transition states that are difficult to locate. For the C−O homolysis reaction, (1) and (7), we used the A from reactions 18 and 19. Experimental A factors for reaction 18 vary from[51,62−65] 1×10^{15} to 1×10^{16} s^{-1}, while the experimental A for reaction 19 varies[18,66,67] from 2×10^{14} to 5×10^{15} s^{-1}. We have used the value from Arends et al.,[64] $A_{(1)} = A_{(7)} = 2 \times 10^{15}$ s^{-1}. For C−C homolysis, reaction 21, experimental A values[55,68−73] varied from 4×10^{14} to 9×10^{15} s^{-1}. We use the A value from Muller-Markgraf et al.,[55] $A_{(21)} = 4 \times 10^{15}$ s^{-1}.

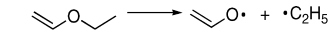

(20)

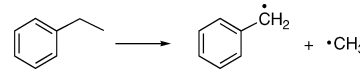

(21)

For the concerted reactions, we determined the activation energy and pre-exponential factors by the method described in the Computation section (vide supra) and eqs 1−4. The molecular structures for the transition states obtained with B3LYP/6-311(d,p) are shown in Figure 8, where bond lengths from the reaction coordinate are called out. For comparison of reactions 5 and 6 with previous experimental values, we refit the calculated results using a simple Arrhenius expression ($k(T) = A\ e^{-E_a/(RT)}$, that is, $n = 0$ in eq 4). Using this method we obtained a value of $A_{(5)} = 1.3 \times 10^{12}$ s^{-1}, while the experimental values[17,74,75] are 2.9×10^{11}, 6.7×10^{11}, and 1.2×10^{12} s^{-1}. The calculated pre-exponential factor for reaction 6 is $A_{(6)} = 1.5 \times 10^{14}$ s^{-1}, while the experimental values[18,67] are 1.0×10^{13} and 7.9×10^{13} s^{-1}. Figure 8 also collects the molecular geometries for the retro-ene and Maccoll transition states for PPE and PEE. As can be seen, bond lengths for the reaction coordinates are similar. The calculated A factors and activation energies for the concerted reactions for PPE and PEE (reactions 3, 4, 7, and 9) are also collected in Table 3. Using the parameters from this table, rate constants can be calculated and Figure 9 plots these as a function of temperature.

As Figure 9 shows, the rate constants for the four reaction channels for PPE, reactions 1−4, are more closely spread than the rate constants estimated in Figure 1. Over the entire temperature range the C−C homolysis reaction is slow compared to the other three reactions, accounting for less than 2% of the PPE loss rate. As Table 3 shows, the calculated activation energies for the homolysis reactions, (1) and (2), and the Maccoll elimination, (4), are only slightly higher than the predicted values used for Figure 1, while the activation energy for the retro-ene reaction, (3), is 10 kcal mol^{-1} higher than the estimated value. As a result, the rate constant for the retro-ene reaction is closer to the other channels. At low temperatures it is still about 2 orders of magnitude higher than the rate constant for the C−O homolysis reaction and about 5× higher than the Maccoll reaction at 500 °C. Hence, the calculations confirm the estimates in that the retroene reaction is the dominant low temperature channel. As temperature increases both the Maccoll and C−O homolysis reactions increase faster than the retro-ene rate

TABLE 3: Arrhenius Rate Parameters

reaction	$k(T) = AT^n e^{-E/(RT)}$			$k(T) = A e^{-E_a/(RT)}$	
	A (s^{-1})	n	E (kcal mol^{-1})	A	E_a (kcal mol^{-1})
$CH_3CH_2OCHCH_2 \rightarrow C_2H_4 + CH_3CHO$	1.0×10^8	1.2	44[a]	1.5×10^{12}	46
$(CH_3CH_2)_2O \rightarrow C_2H_5OH + C_2H_4$	1.9×10^6	2.3	64[b]	1.8×10^{14}	69
PPE $\rightarrow C_6H_6CH_2CH_2^{\bullet} + C_6H_5O^{\bullet}$	2×10^{15}		68[b]	2×10^{15}	68
PPE $\rightarrow C_6H_6CH_2^{\bullet} + C_6H_5OCH_2^{\bullet}$	4×10^{15}		78[b]	4×10^{15}	78
PPE $\rightarrow$ styrene + CHD (**8**)	2.2×10^6	1.9	49[a]	8.7×10^{12}	53
PPE $\rightarrow$ styrene + phenol	2.1×10^8	1.9	59[a]	8.3×10^{14}	63
PPE $\rightarrow C_6H_5O^{\bullet} + C_2H_5^{\bullet}$	2×10^{15}		67[b]	2×10^{15}	67
PPE $\rightarrow$ CHD (**8**) + C_2H_4	5.5×10^7	1.6	54[a]	2.0×10^{13}	57
PPE $\rightarrow$ phenol + C_2H_4	2.1×10^8	1.8	62[a]	3.7×10^{14}	66

[a] Parameters for eq 2 were determined using CBS-QB3 calculations and fit to a modified Arrhenius equation (eq 4). [b] See text.

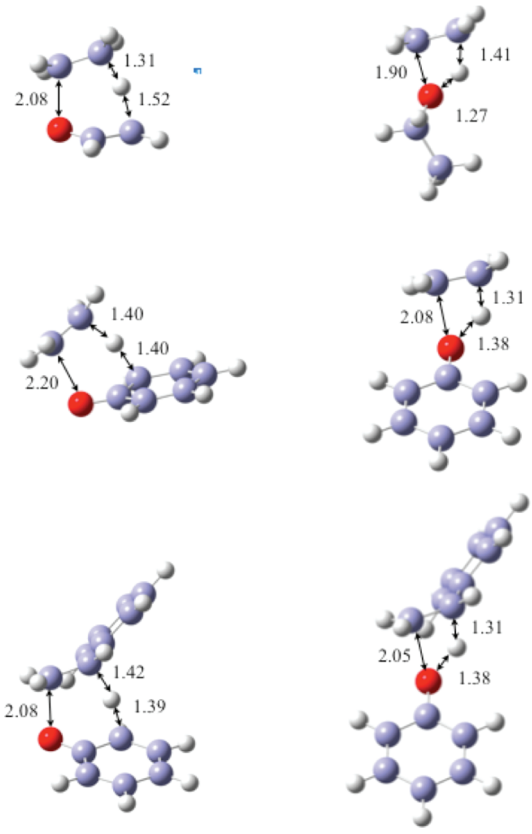

Figure 8. Molecular geometries of the transition states for reactions 5, 6, 8, 9, 3, and 4 as determined using B3LYP/6-311(d,p).

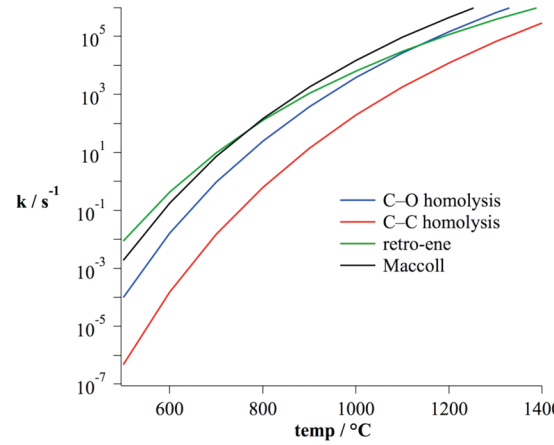

Figure 9. Calculated rate constants for reactions 1−4 based upon results from CBS-QB3 calculations (see Table 3 for rate parameters).

constant. However, at temperatures greater than 800 °C these three reactions have rate constants predicted to be within a factor of 5 of each other, which is within the uncertainty of the theoretical method used here and the estimation of the pre-exponential factors. Due to these high uncertainties, a firm prediction of the relative importance of the different channels is at this point impossible. The predominance of products from the homolysis reaction would suggest that the estimated rate expression of this reaction might be too low. Note that the highest rate constants shown in Figure 9 reach values on the order of 1×10^3 to 1×10^4 s^{-1} at 900 °C, which translates to life times in the order of hundreds of microseconds. Given some uncertainties of the temperature inside of the tubular reactor, these values agree well with Figures 3 and 4, which show that PPE pyrolysis products were observed at temperatures above 800 °C.

In the PEE system, the retro-ene reaction still dominates at low temperatures (<800 °C) but the Maccoll reaction is about a factor of 2−3 lower than the C−O homolysis reaction over the entire temperature range (see Supporting Information for a figure comparing the rate constants). These results are consistent with the experimental observations, which suggest that the C−O homolysis products (*m/z* 93 and 65) begin to appear at temperatures higher than 1000 °C, whereas the concerted reactions dominate at lower temperatures.

Conclusions

This is the first study to directly observe products for reactions 1−4 for the pyrolysis of PPE. Radical and stable products were detected using PIMS for PPE and PIMS and matrix-IR for PEE. For the PPE system, observations of phenoxy radical, cyclopentadienyl radical, benzyl radical, styrene, and benzene were indicative of homolysis of the CO and CC bonds (reactions 1 and 2), whereas detection of phenol and styrene suggest pyrolysis by concerted reactions (reactions 3 and 4). Experimental results, supported by theoretical calculations, indicate that the C−O homolysis (reaction 1) is significant at high temperatures (>1000 °C), whereas the concerted "retro-ene" and Maccoll mechanisms (reactions 3 and 4) are significant at lower temperatures. The C−C homolysis mechanism (reaction 2) is minor at all temperatures. These results indicate that under typical pyrolytic conditions ($T < 600$ °C) the concerted reactions will dominate over homolytic pathways. However, radical products from the homolytic reactions have been linked to aromatic growth formation and will likely lead to tar formation

at higher concentrations and longer pyrolysis times. Due to the recalcitrant nature of tars and the impact radical products can have on product distribution, the homolytic reactions, although minor, must be considered even at low temperatures.

Acknowledgment. This work was supported by the U.S. Department of Energy's Biomass Program, under Contract No. DE-AC36-99GO10337 with the National Renewable Energy Laboratory. We would like to thank Professor G. Barney Ellison, Angayle Vasiliou, and Adam M. Scheer, University of Colorado, and Calvin Mukarakate, National Renewable Energy Laboratory.

Supporting Information Available: Cartesian coordinates of all structures used in our kinetic analysis are provided in the Supporting Information. We also provide kinetic modeling plot for PEE, benzene production from styrene pyrolysis alone and during PPE experiments, matrix-IR spectra of PEE pyrolysis at high (1:500) and low (1:1000) concentration. This material is available free of charge via the Internet at http://pubs.acs.org.

References and Notes

(1) Brenzy, R.; Mihalov, V.; Kvacik, V. *Holzforschung* **1983**, *37*, 199.
(2) Jegers, H. E.; Klein, M. T. *Ind. Eng. Chem. Prod. Res. Dev.* **1985**, *24*, 173.
(3) Klein, M. T.; Virk, P. S. Modeling of Lignin Thermolysis. *MIT Energy Laboratory Report No. MIT-EL 81-005* 1981.
(4) Klein, M. T.; Virk, P. S. *Ind. Eng. Chem. Fund.* **1983**, *22*, 35.
(5) Bridgwater, T. *J. Sci. Food Agric.* **2006**, *86*, 1755.
(6) Evans, R. J.; Milne, T. A.; Soltys, M. N. *J. Anal. Appl. Pyrolysis* **1986**, *9*, 207.
(7) Hoffmann, H. M. R. *Angew. Chem., Int. Ed. Engl.* **1969**, *8*, 556.
(8) Maccoll, A. *Chem. Rev.* **1969**, *69*, 33.
(9) Britt, P. F.; Buchanan, A. C.; Cooney, M. J.; Martineau, D. R. *J. Org. Chem.* **2000**, *65*, 1376.
(10) Britt, P. F.; Buchanan, A. C.; Malcolm, E. A. *J. Org. Chem.* **1995**, *60*, 6523.
(11) Stein, S. E.; Brown, R. L. Structures and Properties Group Additivity Model. In *NIST Chemistry WebBook, NIST Standard Reference Database No. 69*; Linstrom, P. J., Mallard, W. G., Eds.; National Institute of Standards and Technology: Gaithersburg MD, 20899, 2010.
(12) The enthalpy of formation of PPE, **1**, can be calculated using Benson's group additivity method (ref 11) as $\Delta_f H_{298}(C_6H_5C_2H_4OC_6H_5) = 1.7$ kcal mol^{-1}. Assuming the C−H bond enthalpy for ethylbenzene is similar to ethane, $DH_{298}(CH_3CH_2-H) = 101.1 \pm 0.4$ kcal mol^{-1},[15] and using the heat of formation for ethylbenzene, $\Delta_f H_{298}(C_6H_5CH_2CH_3) = 7.2 \pm 0.2$ kcal mol^{-1},[13] and heat of formation of the hydrogen atom, $\Delta_f H_{298}(H) = 52.103 \pm 0.003$ kcal mol^{-1},[14] the calculated heat of formation for the 2-phenylethyl radical, **2**, is calculated to be $\Delta_f H_{298}(C_6H_5C_2H_4) = 79$ kcal mol^{-1}. The heat of formation of the phenoxy radical, **3**, has been determined by Angel and Ervin[16] to be $\Delta_f H_{298}(C_6H_5O) = 11 \pm 1$ kcal mol^{-1}. These values are used to estimate the C−O bond homolysis enthalpy for reaction 1. The enthalpy for the C−C bond homolysis enthalpy for reaction 2 can be estimated from the heat of formation of the benzyl radical, $\Delta_f H_{298}(C_6H_5CH_2) = 49.7 \pm 0.6$ kcal mol^{-1},[17] and the heat of formation of the phenoxymethyl radical $C_6H_5OCH_2$. This heat of formation can be estimated using the C−H bond dissociation enthalpy of ethane and the heat of formation of anisole, $\Delta_f H_{298}(C_6H_5OCH_3) = -16.2 \pm 2.6$ kcal mol^{-1},[13] giving a value of $\Delta_f H_{298}(C_6H_5OCH_2) = 33$ kcal mol^{-1}.
(13) Pedley, J. B. *Thermochemical Data and Structures of Organic Compounds*; Thermodynamics Research Center: College Station, TX, 1994; Vol. I.
(14) Gurvich, L. V.; I.V., V.; Alcock, C. B.; Iorish, V. S. *Thermodynamic Properies of Individual Substances*, 4th ed.; Hemisphere: New York, 1991; Vol. 2.
(15) Seakins, P. W.; Pilling, M. J.; Niiranen, J. T.; Gutman, D.; Krasnoperov, L. N. *J. Phys. Chem.* **1992**, *96*, 9847.
(16) Angel, L. A.; Ervin, K. M. *J. Phys. Chem. A* **2004**, *108*, 8346.
(17) Ellison, G. B.; Davico, G. E.; Bierbaum, V. M.; DePuy, C. H. *Int. J. Mass Spectrom. Ion Processes* **1996**, *156*, 109.
(18) Shimofuji, K.; Saito, K.; Imamura, A. *J. Phys. Chem.* **1991**, *95*, 155.
(19) Seres, I.; Huhn, P. *Magyar Kemiai Folyoirat* **1975**, *81*, 120.
(20) Friderichsen, A. V.; Radziszewski, J. G.; Nimlos, M. R. *J. Am. Chem. Soc.* **2001**, *123*, 1977.
(21) Rohrs, H. W.; Wickhamjones, C. T.; Ellison, G. B.; Berry, D.; Argrow, B. M. *Rev. Sci. Instrum.* **1995**, *66*, 2430.
(22) Vasiliou, A.; Nimlos, M. R.; Daily, J. W.; Ellison, G. B. *J. Phys. Chem. A* **2009**, *113*, 8540.
(23) Zhang, X.; Friderichsen, A. V.; Nandi, S.; Ellison, G. B.; David, D. E.; McKinnon, J. T.; Lindeman, T. G.; Dayton, D. C.; Nimlos, M. R. *Rev. Sci. Instrum.* **2003**, *74*, 3077.
(24) Chen, P.; Cy, I. N.; Baer, T.; Powis, I. *Unimolecular and bimolecular reaction dynamics*; Wiley: New York, 1994.
(25) Nandi, S.; Blanksby, S. J.; Zhang, X.; Nimlos, M. R.; Dayton, D. C.; Ellison, G. B. *J. Phys. Chem. A* **2002**, *106*, 7547.
(26) Nandi, S.; Arnold, P. A.; Carpenter, B. K.; Nimlos, M. R.; Dayton, D. C.; Ellison, G. B. *J. Phys. Chem. A* **2001**, *105*, 7514.
(27) Zhang, X.; Maccarone, A. T.; Nimlos, M. R.; Kato, S.; Bierbaum, V. M.; Ellison, G. B.; Ruscic, B.; Simmonett, A. C.; Allen, W. D.; Schaefer, H. F. *J. Chem. Phys.* **2007**, *126*, 044312.
(28) Friderichsen, A. V.; Shin, E. J.; Evans, R. J.; Nimlos, M. R.; Dayton, D. C.; Ellison, G. B. *Fuel* **2001**, *80*, 1747.
(29) Jochnowitz, E.; Zhang, Nimlos; Flowers, B.; Stanton, Ellison. *J. Phys. Chem. A* **2010**, *114*, 1498.
(30) Jochnowitz, E. B.; Zhang, X.; Nimlos, M. R.; Varner, M. E.; Stanton, J. F.; Ellison, G. B. *J. Phys. Chem. A* **2005**, *109*, 3812.
(31) Brown, A. L.; Dayton, D. C.; Nimlos, M. R.; Daily, J. W. *Chemosphere* **2001**, *42*, 663.
(32) Reid, R. C.; Prausnitz, J. N.; Poling, B. E. *The Properties of Gases and Liquids*, 4th ed.; McGraw-Hill: New York, 1987.
(33) Frisch, M. J.; Trucks, G. W.; Schlegel, H. B.; Scuseria, G. E.; Robb, M. A.; Cheeseman, J. R.; Montgomery, J. A., Jr.; Vreven, T.; Kudin, K. N.; Burant, J. C.; Millam, J. M.; Iyengar, S. S.; Tomasi, J.; Barone, V.; Mennucci, B.; Cossi, M.; Scalmani, G.; Rega, N.; Petersson, G. A.; Nakatsuji, H.; Hada, M.; Ehara, M.; Toyota, K.; Fukuda, R.; Hasegawa, J.; Ishida, M.; Nakajima, T.; Honda, Y.; Kitao, O.; Nakai, H.; Klene, M.; Li, X.; Knox, J. E.; Hratchian, H. P.; Cross, J. B.; Bakken, V.; Adamo, C.; Jaramillo, J.; Gomperts, R.; Stratmann, R. E.; Yazyev, O.; Austin, A. J.; Cammi, R.; Pomelli, C.; Ochterski, J. W.; Ayala, P. Y.; Morokuma, K.; Voth, G. A.; Salvador, P.; Dannenberg, J. J.; Zakrzewski, V. G.; Dapprich, S.; Daniels, A. D.; Strain, M. C.; Farkas, O.; Malick, D. K.; Rabuck, A. D.; Raghavachari, K.; Foresman, J. B.; Ortiz, J. V.; Cui, Q.; Baboul, A. G.; Clifford, S.; Cioslowski, J.; Stefanov, B. B.; Liu, G.; Liashenko, A.; Piskorz, P.; Komaromi, I.; Martin, R. L.; Fox, D. J.; Keith, T.; Al-Laham, M. A.; Peng, C. Y.; Nanayakkara, A.; Challacombe, M.; Gill, P. M. W.; Johnson, B.; Chen, W.; Wong, M. W.; Gonzalez, C.; Pople, J. A. *Gaussian 03*, revision C.02; Gaussian, Inc.: Wallingford, CT, 2003.
(34) Montgomery, J. A.; Frisch, M. J.; Ochterski, J. W.; Petersson, G. A. *J. Chem. Phys.* **1999**, *110*, 2822.
(35) Hodgson, D.; Zhang, H. Y.; Nimlos, M. R.; McKinnon, J. T. *J. Phys. Chem. A* **2001**, *105*, 4316.
(36) Nimlos, M. R.; Blanksby, S. J.; Ellison, G. B.; Evans, R. J. *J. Anal. Appl. Pyrolysis* **2003**, *66*, 3.
(37) Nimlos, M. R.; Blanksby, S. J.; Qian, X. H.; Himmel, M. E.; Johnson, D. K. *J. Phys. Chem. A* **2006**, *110*, 6145.
(38) Nimlos, M. R.; Qian, X. H.; Davis, M.; Himmel, M. E.; Johnson, D. K. *J. Phys. Chem. A* **2006**, *110*, 11824.
(39) Beste, A.; Buchanan, A. C. *Energy Fuels* **2010**, *24*, 2857.
(40) Beste, A.; Buchanan, A. C. *J. Org. Chem.* **2009**, *74*, 2837.
(41) Evans, M. G.; Polanyi, M. *Trans. Faraday Soc.* **1935**, *31*, 875.
(42) Eyring, H. *J. Chem. Phys.* **1935**, *3*, 107.
(43) Curtiss, L. A.; Raghavachari, K.; Redfern, P. C.; Pople, J. A. *J. Chem. Phys.* **1997**, *106*, 1063.
(44) Pertersson, G. A.; Malick, D. K.; Wilson, W. G.; Ochterski, J. W.; Montgomery, J. A., Jr.; Frisch, M. J. *J. Chem. Phys.* **1998**, *109*, 10570.
(45) Pitzer, K. S.; Gwinn, W. D. *J. Chem. Phys.* **1942**, *10*, 428.
(46) Kilpatrick, J. E.; Pitzer, K. S. *J. Chem. Phys.* **1949**, *17*, 1064.
(47) East, A. L. L.; Radom, L. *J. Chem. Phys.* **1997**, *106*, 6655.
(48) Eckart, C. *Phys. Rev.* **1930**, *35*, 1303.
(49) The enthalpy of reaction 10 can be determined from the heat of formation of 2-phenylethyl radical, **2**,[12] the heat of formation of styrene, $\Delta_f H_{298}(C_6H_5C_2H_3) = 35.4 \pm 0.3$ kcal mol^{-1},[13] and the heat for formation of the hydrogen atom..[14]
(50) Erman, P.; Karawajczyk, A.; Rachlew-Kallne, E.; Stromholm, C.; Larsson, J.; Persson, A.; Zerne, R. *Chem. Phys. Lett.* **1993**, *215*, 173.
(51) Lin, C. Y.; Lin, M. C. *J. Phys. Chem.* **1986**, *90*, 425.
(52) Scheer, A. M.; Mukarakate, C.; Robichaud, D. J.; Ellison, G. B.; Nimlos, M. R. *J. Phys. Chem. A* **2010**, *114*, 13.
(53) Carlier, P.; Dubois, J. E.; Masclet, P.; Mouvier, G. *J. Electron Spectrosc. Relat. Phenom.* **1975**, *7*, 55.
(54) Moskaleva, L. V.; Lin, M. C. *J. Comput. Chem.* **2000**, *21*, 415.
(55) Muller-Markgraf, W.; Troe, J. *J. Phys. Chem.* **1988**, *92*, 4914.
(56) Mulcahy, Tucker; Williams, Wilmshurst *Aust. J. Chem.* **1967**, *20*, 1155.
(57) Xia, W. S.; Lin, M. C. *Phys. Chem. Chem. Phys.* **2000**, *2*, 5566.
(58) Robichaud, D. J.; Hansen, J. C.; Kumbhani, S.; Nimlos, M. R. *J. Phys. Chem. A*, manuscript in preparation.
(59) Lias, S. G. Ionization Energy Evaluation. In *NIST Chemistry WebBook, NIST Standard Reference Database No. 69*; Linstrom, P. J.,

Mallard, W. G., Eds.; National Institute of Standards and Technology: Gaithersburg MD, 20899, 2010.

(60) Zhu, L.; Bozzelli, J. W. *J. Phys. Chem. A* **2003**, *107*, 3696.

(61) Williams, B. A.; Cool, T. A. *J. Chem. Phys.* **1991**, *94*, 6358.

(62) Mackie, J. C.; Doolan, K. R.; Nelson, P. F. *J. Phys. Chem.* **1989**, *93*, 664.

(63) Suryan, M. M.; Kafafi, S. A.; Stein, S. E. *J. Am. Chem. Soc.* **1989**, *111*, 1423.

(64) Arends, I. W. C. E.; Louw, R.; Mulder, P. *J. Phys. Chem.* **1993**, *97*, 7914.

(65) Bruinsma, O. S. L.; Geertsma, R. S.; Bank, P.; Moulijn, J. A. *Fuel* **1988**, *67*, 327.

(66) Seres, I.; Labadi, I.; Huhn, P. *Magyar Kemiai Folyoirat* **1977**, *83*, 151.

(67) Foucaut, J. F.; Martin, R. *J. Chim. Phys. Phys.-Chim. Biol.* **1978**, *75*, 132.

(68) Mizerka, L. J.; Kiefer, J. H. *Int. J. Chem. Kinet.* **1986**, *18*, 363.

(69) Esteban, G. L.; Kerr, J. A.; Trotman-Dickenson, A. F. *J. Chem. Soc.* **1963**, 3873.

(70) Crowne, C. W. P.; Grigulis, V. J.; Throssell, J. J. *J. Chem. Soc., Faraday Trans.* **1969**, *65*, 1051.

(71) Clark, W. D.; Price, S. J. *Can. J. Chem.* **1970**, *48*, 1059.

(72) Robaugh, D. A.; Stein, S. E. *Int. J. Chem. Kinet.* **1981**, *13*, 445.

(73) Grela, M. A.; Colussi, A. J. *Int. J. Chem. Kinet.* **1985**, *17*, 257.

(74) Rossi, M.; Golden, D. M. *Int. J. Chem. Kinet.* **1979**, *11*, 715.

(75) McEwen, I.; Taylor, R. *J. Chem. Soc., Perkins Trans. 2* **1982**, 1179.

(76) Gray, P.; Williams, A. *Trans. Faraday Soc.* **1959**, *55*, 760.

(77) Ruscic, B.; Boggs, J. E.; Burcat, A.; Csaszar, A. G.; Demaison, J.; Janoschek, R.; Martin, J. M. L.; Morton, M. L.; Rossi, M. J.; Stanton, J. F.; Szalay, P. G.; Westmoreland, P. R.; Zabel, F.; Berces, T. IUPAC critical evaluation of thermochemical properties of selected radicals. Part I. *J. Phys. Chem. Ref. Data* **2005**, *34*, 573.

(78) The C−O bond dissociation energy for anisole can be determined from the heat of formation of anisole $\Delta_f H_{298}(C_6H_5OCH_3) = -16.2 \pm 2.6$ kcal mol^{-1},[13] the heat of formation of the phenoxy radical,[16] and the heat of formation of the methyl radical $\Delta_f H_{298}(CH_3) = 35.05 \pm 0.02$ kcal mol^{-1}.[84]

(79) Pilcher, G.; Skinner, H. A.; Pell, A. S.; Pope, A. E. *Trans. Faraday Soc.* **1963**, *59*, 316.

(80) Berkowitz, J.; Ellison, G. B.; Gutman, D. *J. Phys. Chem.* **1994**, *98*, 2744.

(81) The C−O dissociation enthalpy of vinyl ethyl ether dissociationcan be determined from the heat of formation of this molecule, $\Delta_f H_{298}(C_2H_5OC_2H_3) = -33.5 \pm 0.2$ kcal mol^{-1},[79] the heat of formation of ethyl radical, $\Delta_f H_{298}(C_2H_5) = 29.0 \pm 0.4$ kcal mol^{-1},[15] and the heat of formation of the vinoxy radical, $\Delta_f H_{298}(C_2H_3O) = 2.5 \pm 2.2$ kcal mol^{-1}.[80]

(82) Ervin, K. M.; DeTuro, V. F. *J. Phys. Chem. A* **2002**, *106*, 9947.

(83) The C−O dissociation enthalpy of diethyl ether can be determined from the enthalpy of formation of this molecule, $\Delta_f H_{298}(C_2H_5OC_2H_5) = -64.4 \pm 0.5$ kcal mol^{-1},[13] the heat of formation of ethyl radical, $\Delta_f H_{298}(C_2H_5) = 29.0 \pm 0.4$ kcal mol^{-1},[15] and the heat of formation of ethoxy radical, $\Delta_f H_{298}(C_2H_3O) = 2.5 \pm 2.2$ kcal mol^{-1}.[82]

(84) Ruscic, B.; Litorja, M.; Asher, R. L. *J. Phys. Chem. A* **1999**, *103*, 8625.

(85) The C−C dissociation enthalpy of ethylbenzene can be determined from the heat of formation of this molecule, $\Delta_f H_{298}$ $(C_6H_5CH_2CH_3) = 7.2 \pm 0.2$ kcal mol^{-1},[13] the heat of formation of benzyl radical, $\Delta_f H_{298}(C_6H_5CH_2) = 49.7 \pm 0.6$ kcal mol^{-1},[17] and the heat of formation of methyl radical, $\Delta_f H_{298}(C_6H_5CH_2) = 35.05 \pm 0.07$ kcal mol^{-1}.[84]

(86) Holmes, J. L.; Lossing, F. P.; Mayer, P. M. *J. Am. Chem. Soc.* **1991**, *113*, 9723.

(87) The C−C dissociation enthalpy for diethyl ether can be determined from the heat of formation of this molecule, $\Delta_f H_{298}(C_2H_5OC_2H_5) = -64.4 \pm 0.5$ kcal mol^{-1},[13] the heat of formation of ethoxy methyl radical, $\Delta_f H_{298}(C_2H_5OCH_2{-}CH_3$ dissociation$) = -10.6$ kcal mol^{-1},[86] and the heat of formation of the methyl radical, $\Delta_f H_{298}(C_6H_5CH_2) = 35.05 \pm 0.07$ kcal mol^{-1}.[84]

(88) Spanget-Larsen, J.; Gil, M.; Gorski, A.; Blake, D. M.; Waluk, J.; Radziszewski, J. G. *J. Am. Chem. Soc.* **2001**, *123*, 11253.

(89) Michalska, D.; Zierkiewicz, W.; Bienko, D. C.; Wojciechowski, W.; Zeegers-Huyskens, T. *J. Phys. Chem. A* **2001**, *105*, 8734.

(90) Coleman, W. M.; Gordon, B. M. *Appl. Spectrosc.* **1989**, *43*, 1008.

(91) Barnes, A. J.; Howells, J. D. R. *J. Chem. Soc., Faraday Trans. II* **1973**, 532.

(92) Korolev, V. A.; Nefedov, O. M. *Russ. Chem. Bull.* **1993**, *42*, 1436.

(93) Davies, J. B.; Hallam, H. E. *J. Chem. Soc., Faraday Trans. II* **1972**, *68*, 509.

(94) Engdahl, A.; Nelander, B. *Chem. Phys. Lett.* **1983**, *100*, 129.

JP1076356